Science of the Total Environment 708 (2020) 134516

Contents lists available at ScienceDirect

Science of the Total Environment

journal homepage: www.elsevier.com/locate/scitotenv

Short communication

# Relationship between pedestrian-level outdoor thermal comfort and building morphology in a high-density city

Ka-Ming Wai [a,d,*,1], Chao Yuan [a], Alan Lai [b], Peter K.N. Yu [c]

[a] Department of Architecture, School of Design and Environment, National University of Singapore, Singapore
[b] School of Architecture, Chinese University of Hong Kong, Hong Kong Special Administrative Region
[c] Department of Physics, City University of Hong Kong, Hong Kong Special Administrative Region
[d] Intelligent Manufacturing Key Laboratory of Ministry of Education, Shantou University, China

## HIGHLIGHTS

- We quantified the relationship between urban forms and thermal comfort.
- Our CFD and thermal comfort models were validated by measurements.
- Our coupled model produced comparable $T_{mrt}$ and sensible *PET* relative to other studies.
- Predicted *PETs* at noon were more than 10 °C relative to the morning within buildings.
- Modifications of building lengths and porosity were keys to reduce heat stresses.

## GRAPHICAL ABSTRACT

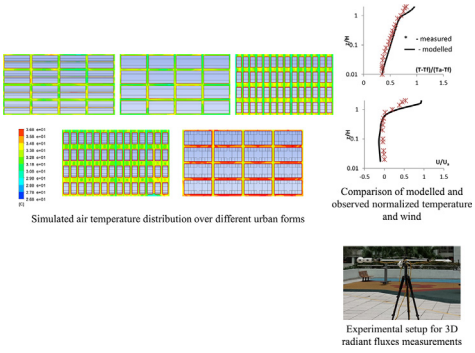


## ARTICLE INFO

*Article history:*
Received 17 April 2019
Received in revised form 16 September 2019
Accepted 16 September 2019
Available online 8 October 2019

Editor: Scott Sheridan

*Keywords:*
Heat stress
Urban climate modeling
Urban sustainability
Computational fluid dynamics

## ABSTRACT

Urban compact buildings impose large frictional drag on boundary-layer air flow and create stagnant air within the building environment. It results in exacerbating the street-level outdoor thermal comfort (OTC). It is common to perform in-situ measurements of the OTC in different urban forms and to study their relationship. However, it is impossible to do so from a planning perspective because of the absence of physical planned urban forms. Our objective was to quantify the thermal environment and OTC in different planned complex urban forms by well-validated numerical models. We coupled a computational fluid dynamics (CFD) model to an OTC (Rayman) model to study the OTC. The κ–ω SST turbulent model was adopted for the CFD simulations, with accuracy of the turbulent model validated by wind tunnel measurements. The highest calculated air temperature within the street canyon of a planned bulky urban form could reach more than 5 °C higher than the surrounding environment. Within the tested urban forms, our coupled model predicted mean radiant temperature comparable with measurements in the literature. The model also produced sensible street-level physiologically equivalent temperatures (*PETs*) when comparing with those listed in the human thermal sensation categories. In the morning, the predicted *PETs* within all the urban forms were lower than that in open areas, which indicated that the shading of buildings effectively reduced the *PET* increase due to solar irradiance. At noon, increases in *PETs* by more than 10 °C relative to the morning situation indicated that when the buildings acted as heat sources after insolation absorption, increase in the air temperature at the street intersection and in the

* Corresponding author.
*E-mail address:* jmwei@stu.edu.cn (K.-M. Wai).
[1] Now in the Department of Civil and Environmental Engineering, Shantou University, China.

https://doi.org/10.1016/j.scitotenv.2019.134516

street canyon made an important contribution to the receiver *PETs*. The reduction in building lengths and increase in the low-level porosity were the most effective ways to reduce the heat stress at the pedestrian-level.



## 1. Introduction

The study of the relationship between the urban heat island (UHI) and outdoor thermal comfort (OTC) is important (see e.g. Rose, 2010; Steeneveld et al., 2011; van Hove et al., 2015; Hiemstra et al., 2017) but the UHI and OTC are often implicitly linked (van Hove et al., 2015). The UHI effect causes urban areas to have higher air temperatures than those in rural surroundings [on average 5 °C higher for Asian and Australian cities (Santamouris, 2015)], and thus worsens the OTC in urban areas. Two major factors that determine the OTC are the wind speed and air temperature (van Hove et al., 2015; Morabito et al., 2014; Guéritée and Tipton, 2015; Hiemstra et al., 2017; Yang et al., 2017), while building morphology has significant impacts on these factors.

Firstly the relationship between building morphology and wind was discussed. With computational fluid dynamics (CFD) models, we investigated the relationship between building porosity and urban ventilation in search of better building forms (Yuan and Ng, 2012) and dispersion potential in a complex urban form (Chu et al., 2005). Asfour (2010) found that a group of buildings with a central opening space in between offered better wind exposure and containment using a CFD model. Based on the wind measurements and building information, Yang et al. (2013) reported that an increase in the sky view factor (SVF) by 10% could increase the wind velocity ratio (WVR) by 7–8% in a high-rise built environment, where the WVR was the ratio of wind velocity at the pedestrian level to that of the unobstructed wind.

The building morphology also has major effects on the thermal environment. A study in Italy using a building height of 14 m concluded that a higher building density (53 versus 32 buildings in the same area) led to an increase in the air temperature by 1 °C (Perini and Magliocco, 2014). Allegrini et al. (2015) studied the air temperature distribution over different building morphologies (simple cubical buildings arrangements) through a CFD model – OpenFOAM, and found higher air temperatures inside the building arrays of up to 2.5 °C relative to the surrounding for all cases. A linear relationship was also revealed between the average air temperature and a quantity which measured the distance the wind could flow freely until hitting a building wall. Based on an OTC model - ENVI-met model, positive linear relationships were established between the SVF and the mean radiant temperature ($T_{mrt}$; $r^2$ = 0.57) and the air temperature ($r^2$ = 0.41) at mid-day in Toronto, Canada as a consequence of strong exposure to insolation (Wang et al., 2016). This implied that tall buildings reduced the SVF by increasing the amount of shading at the street-level and thus leading to cooling there. The same model predicted differences in the physiologically equivalent temperature (*PET*) between deep and shallow canyons of more than 20 °C in Singapore (Yang et al., 2015).

In real-life situations, it is common to perform in-situ measurements of street-level OTC in different urban forms and to study their relationship. However, in-situ measurements are impossible from a planning perspective because of the absence of physical planned urban forms. Furthermore, prediction of wind and air temperature within areas of complex urban forms is not offered by common available OTC models. To resolve the issues, the objectives of the present study were therefore to use well-validated numerical models to (1) quantify the thermal environment in different existing and planned complex urban forms, and (2) investigate the relationship between the OTC and urban forms of a high-density city. The current study focused on the thermal environment and OTC while the study by Yuan and Ng (2012) focused on the wind environment only.

## 2. Method

### 2.1. Urban forms being studied

Five representative urban forms in Mong Kok, Hong Kong (22.33°N, 114.16°E) were selected to test the effects of different building morphologies on the OTC at pedestrian level. The urban forms (Cases 1, 2, 5, 6a and 7) with significantly different morphological designs were detailed and illustrated in Yuan and Ng (2012), which represented the present and future urban forms in Hong Kong. The site areas for different cases were the same (200 m × 100 m). Briefly, Case 1 was the present urban form of Mong Kok with a mean population density of 130,000 per $km^2$ (MK, 2019), where the heights of buildings and podiums were on average 60 m and 15 m, respectively. The site was not fully occupied. Podiums are multiple storeys of concrete structures with mixed-use of retail, restaurant, commercial and parking. Case 2 was the future urban form of Mong Kok with the building heights increased to 90 m on average, and the site was fully occupied. Case 5 (building height = 123 m; future urban form) included building setbacks and separation of long buildings. A stepped podium and building void were included in Case 6a (building height = 123 m; future urban form). Air passages were applied to high and wide buildings in Case 7 (building height = 110 m; future urban form) by introducing porosity at building towers and podiums. It was also the major difference in building design between Case 7 and Case 2. However, the porosity was not arranged near the pedestrian level for Case 7. The designs for Cases 5, 6a and 7 were to mitigate the negative wall effects caused by the alignment of long and tall buildings. The building volumes for these cases were similar to that in Case 2. We also added a new case "Open-space", for which no building, no tree, no grass and no other landscape features were included, for comparison with the cases described above.

### 2.2. Setup of CFD model

Numerical air flow and heat transfer simulations for the above cases were performed by a computational fluid dynamics (CFD) model – FLUENT v15.0. The model setup, details and evaluation for wind were described in detail in Yuan and Ng (2012) and summarized in Table 1. Each case consisted of an array (6 × 10) of buildings and two rows of surrounding randomized buildings (Fig. 1). The same regular street grid was applied to all cases with the width of street canyons set as 20 m. Only the calculated wind and temperature data at the innermost area (Fig. 1) were used as model inputs for the RayMan model as discussed in the following. The buildings in the outer area were included to reproduce adequate turbulence kinetic energy in urban areas, which was difficult to achieve under the inlet boundary condition. The computational domain dimensions were 3200 m × 3000 m × 450 m (W × L × H). The grid point numbers, which were case-dependent, were 5.0 –

**Table 1**
The CFD model settings.

| | |
|---|---|
| Computational domain | L × W × H; 3000 m × 3200 m × 450 m |
| Grid expansion ratio | <1.3 |
| Grid resolution | <1/10 of building height |
| Blockage ratio | <5% |
| Grid type | Structural grid |
| Total number of grids | 5.0–6.8 million, case-dependent |
| Inlet boundary condition | See text |
| Outlet boundary condition | Pressure outlet with zero gauge pressure |
| Near wall treatment | No wall function |
| Convergence criteria | <1e−5 |

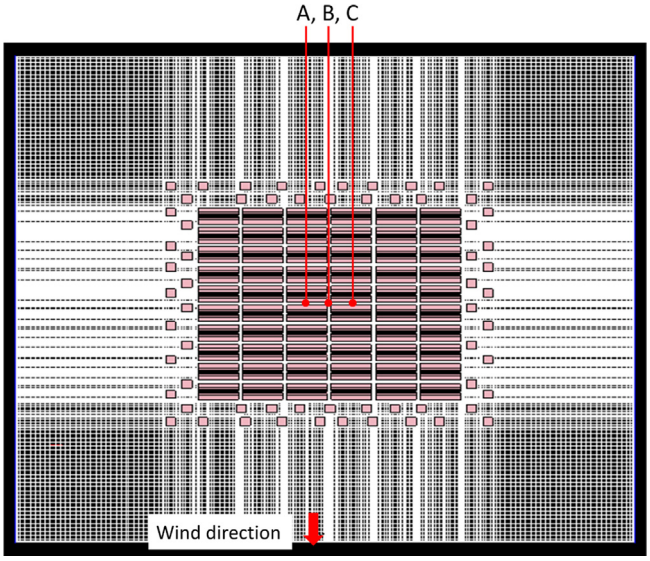


**Fig. 1.** Computational domain and grids. The location of assessment points, building array and randomized block were also presented. Urban form for Case 1 was illustrated as an example.

6.8 million. Finer meshes were arranged in the areas close to the ground with an expansion rate of 1.2. The worst-case scenario was chosen when the prevailing wind was significantly blocked by the buildings (see wind direction shown in Fig. 1). All simulations were performed using the FLUENT model with the κ–ω shear-stress transport (SST) turbulence model (Fluent, 2006; Yuan and Ng, 2012). The κ–ω SST turbulence model is a combination of the standard κ–ω model and κ–ε model. The κ–ω SST turbulence model uses the standard κ–ω model for the simulation in the inner part of the near-wall region and gradually changes to the κ–ε model for the simulation in the outer part (Fluent, 2006; Menter et al., 2003). Two scenarios, namely, "no-heat" and "with-heat", were introduced and simulated for each Case. For the "no-heat" scenario, neutral turbulence flows were simulated by the Reynolds-averaged Navier-Stokes (RANS) equations with the κ–ω SST turbulence model. The simulations and associated model validation were the same as that described in Yuan and Ng (2012). The "with-heat" scenario simulated convective turbulence flows with the mentioned RANS κ–ω SST model, by applying the energy equation to determine the temperature and utilizing the Boussinesq approximation – treating the density change as a function of temperature variation in the momentum equation. The model validation was based on wind tunnel experiments (Uehara et al., 2000) with details discussed in Section 3.1.

*2.2.1. Boundary conditions*

The boundary condition for the inlet wind speed profile was set as:

$$U_z/U_{met} = (Z/Z_{met})^{\alpha} \quad (1)$$

where $U_z$ and $U_{met}$ (11 $ms^{-1}$) were mean wind speeds at height Z and reference height $Z_{met}$ (450 m), respectively, and α was set to 0.35. $U_{met}$ was the site-specific annual wind speed at 450 m above ground obtained from the fifth-generation NCAR/PSU meso-scale model (MM5). The outlet wind profile was set to be the same as the inlet wind profile. For the "with-heat" scenario, to simplify the case the building and ground surface temperature was set to be 15 °C higher than the ground-level air temperature to test the effect of convection, similar approach as adopted in the study of Flaherty et al. (2007). Berdahl and Bretz (1997) reported that, depending on the color and type of material, the surface temperature could be higher than the air temperature by 5–50 °C. In real urban environment, the building rooftops have the highest surface temperature, while the building walls and ground have a spatially varying temperature depending on the sun angle, shading and surface type (Flaherty et al., 2007). Nevertheless, the temperature difference for the "with-heat" scenario was within the range of other studies (Nakamura and Oke, 1988; Louka et al., 2001; Flaherty et al., 2007). The inlet air temperature was set to be 28.1 °C for both "no-heat" and "with-heat" scenarios, which was the 5-year average value measured in the studied area.

*2.3. Setup of RayMan model*

The RayMan model (version 1.2) was adopted to calculate the mean radiant temperature ($T_{mrt}$) and *PET* (Mayer and Höppe, 1987) – as an OTC index. The model description was detailed by Matzarakis et al. (2007, 2010) and Lee and Mayer (2016). The model was previously employed and extensively evaluated for OTC studies, including those in urban built environments (Matzarakis et al., 2007; Andrade and Alcoforado, 2008; Lin et al., 2010; Hwang et al., 2011; Chen et al., 2014; Lee and Mayer, 2016; Wai et al., 2017). The model was further validated in our study. The building forms for different cases were input to the model to calculate the SVF and to take the building shading effects into account. For each case in the "no-heat" scenario, the five-year average of air temperature (28.1 °C) measured at a meteorological station near Mong Kok was input into the RayMan model. The CFD model simulated the wind speed without heating of ground, and building surfaces as described in Section 2.2 were also input into the RayMan model. For the same case in the "with-heat" scenario, the CFD model simulated the wind speed and temperature with heating of ground, and building surfaces described in Section 2.2 were input into the RayMan model. The pedestrian-level (1.1 m above ground) *PETs* at the street intersection (point B) and in the street canyon (points A and C) within the two buildings (Fig. 1) for each case were calculated, after obtaining the mentioned wind and air temperature calculated from the CFD model at these points. The average values at points A and C were adopted for the case of the street canyon. The "no-heat" and "with-heat" scenarios represented situations at 7:00 am and noon, respectively. The *PET* values at these time points were calculated under clear-sky condition at summer solstice. The global radiation was calculated by the model. A person clad with clothing (0.9 clo; a measure of clothing insulation: 1 clo = 0.155 $Km^2W^{-1}$) and having light sedentary activity (80 W) was taken, as a reference human body taken in the *PET* calculation (Mayer and Höppe, 1987) and as model defaults. The human thermal sensation categories reported from a study in Taiwan (23.8°N, 120.9°E; Lin and Matzarakis, 2008) were employed for the current study (Table 2). This represented the best information on *PET* categories available in the literature which was relevant to our study and their study area is "the closest" to ours with similar latitudes.

**Table 2**
Human thermal sensation categories for Hong Kong.

| Thermal sensation | *PET* for Hong Kong[1] (°C) |
|---|---|
| Very cold | <14 |
| Cold | 14 to 18 |
| Cool | 18 to 22 |
| Slightly cool | 22 to 26 |
| Neutral | 26 to 30 |
| Slightly warm | 30 to 34 |
| Warm | 34 to 38 |
| Hot | 38 to 42 |
| Very hot | >42 |

[1] Lin and Matzarakis (2008).

## 3. Model validation

### 3.1. Validation of CFD model for "with-heat" scenario

The validation of the "no-heat" scenario was described in detail in Yuan and Ng (2012), while the validation of the "with-heat" scenario was discussed as follows. A CFD model was set up with a computational domain of 1500 × 6000 × 1000 mm (W × L × H) consisting of an array of 7 × 14 blocks with space in between, to represent simple-shaped building blocks and city streets (Supplementary Information Fig. S1). The unit used in this sub-section was millimeter because of the small size of the domain. The blocks had dimensions of 100 × 100 × 100 mm, which were separated at 100 and 50 mm from each other in the L and W directions, respectively. Fig. S1 also shows the distances (in H, where H is the height of block) between the arrays and various domain boundaries, as well as the sampling location (at the center of the street canyon) where the temperature profile was taken for validation. The sampling location was selected to be the same as that for wind tunnel measurements (Uehara et al., 2000). The boundary conditions at the two sides and the top of the domain were set as "symmetry". No-slip condition was set at the top and side facets of the domain containing the buildings and street canyons. Ten layers were considered for the first 30 mm from the ground with an expansion rate of 1.2, which resulted in a total of about $2 \times 10^6$ computational cells. The model validation compared the results between the wind tunnel experiment and our CFD simulations with the temperature setting and $R_b$ (bulk Richardson number) shown in Table 2 of the work by Uehara et al. (2000). The conditions of $R_b$ = 0.79 (stable), 0.11 and −0.21 (unstable) were used. The inlet wind speed ($U_a$) was set to 1.5 $ms^{-1}$, the same as that for the wind tunnel experiment. Figs. S2 a-c (Figs. S2 d-f) shows good agreement, in particular when z < H, between simulated and measured vertical profiles of non-dimensional normalized temperature (horizontal wind) for different $R_b$ values.

### 3.2. Validation of RayMan model

The simulated $T_{mrt}$ values were compared with the measured values for four different sites during summertime. The measured $T_{mrt}$ values were obtained by integral radiation measurements in real urban environments (Sofia et al., 2007; Lai et al., 2017). The experimental setup of net radiometers was shown in Fig. S3 and detailed in Lai et al. (2017). On the other hand, the simulated $T_{mrt}$ values were obtained by modelling the urban environments using the RayMan model. The simulated and measured $T_{mrt}$ values were compared for four different built environments as shown in Fig. 2 and Table 3. A strong correlation was found between the simulated and measured $T_{mrt}$ values ($r^2$ = 0.85; N = 73), and the ratio between the simulated $T_{mrt}$ to measured $T_{mrt}$ values was found to be 1.16, demonstrating that the RayMan model was an appropriate tool for the simulation of $T_{mrt}$ in urban built environments.

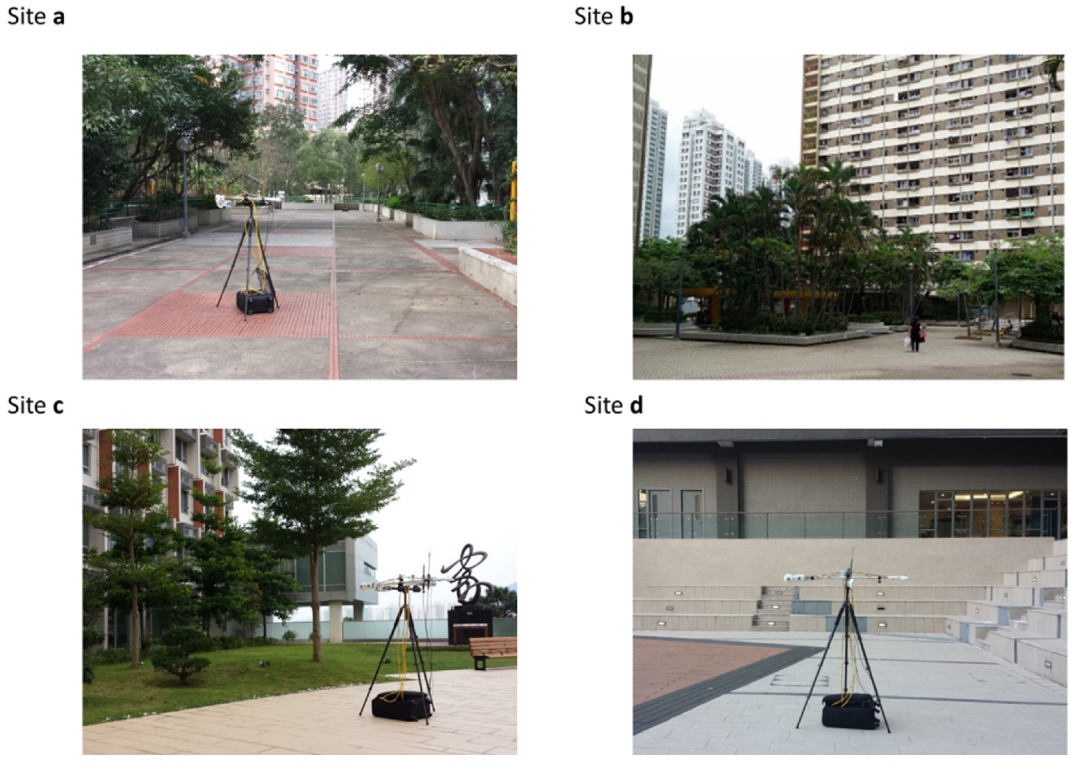


**Fig. 2.** Locations of four different built environments (Sites a – d; description of the Sites referred to Table 3) for mean radiant temperature (°C) measurement for model validation.

## 4. Results and discussion

### 4.1. Calculated air temperature for different cases for "with-heat" scenario

Fig. 3 shows the calculated pedestrian-level air temperatures for the "with-heat" scenario. In general, the air temperatures for Cases 1 and 2 were similar (31 – 35 °C). Despite the higher buildings for Case 2, Case 1 had larger surface areas on the inner sides for each building block. The similar surface areas (as heat sources) for the two cases thus explained the similarity in the temperatures. Relative to Cases 1 and 2, a temperature with 1 °C higher was obtained for Cases 5 and 6a, which was attributed to the higher buildings for the latter cases and thus larger surface areas as heat sources. Since building widths were reduced (comparing with Cases 1 and 2) and gaps between buildings were introduced for Cases 5 and 6a, better air ventilation was achieved at the gaps along with the wind direction. Thus the air temperatures at the gaps along with the wind direction had lower air temperatures. However, the gaps which were perpendicular to the wind direction had higher air temperatures because of the less efficient of air ventilation in these gaps. The building height for Case 7 was similar to those for Cases 5 and 6a. However, a stagnant condition was created for Case 7 due to the building design in such a way that heat was trapped in the street canyon at pedestrian level between the building blocks, when compared to the well-ventilated environments for Cases 5 and 6a. It was noted that poor wind ventilation was reported at the pedestrian level for Case 7 (Yuan and Ng, 2012) and indicated that the porosity design at building towers and podiums did not improve the pedestrian-level wind environment.

**Table 3**
Description of $T_{mrt}$ measurements.

| Site | Description | Duration | Date |
|---|---|---|---|
| a | Common area surrounded by three public residential buildings | 11:00–16:00 | May 29 |
| b | A Courtyard bound by short public residential buildings | 11:00–16:00 | Aug 7 |
| c | A Courtyard near student hostels within a university campus | 15:00–17:00 | Sept 15 |
| d | A Courtyard enclosed by a C-shaped student hostel within a university campus | 15:00–18:00 | Sept 25 |

When comparing the situations for Case 7 and Case 2, Case 7 was found to have more building surfaces (as heat sources) due to the porosity design and building height (31 m higher than Case 2). These resulted in the highest air temperature within the street canyon with temperatures 2 – 3 °C higher than the temperatures obtained from other studied cases. Allegrini et al. (2015) simulated the air temperatures over different building morphologies (simple cubical buildings arrangements). They found that the temperatures in poorly ventilated areas inside the building arrays were up to 2 °C higher than those in well ventilated areas. It was emphasized, however, a direct comparison of the results between their study and our study was difficult since the former adopted different building arrangements and dimensions (10 m height and up to 70 m building width).

### 4.2. Comparison of calculated street-level $T_{mrt}$ and PETs for different urban forms

We compared our $T_{mrt}$ results (Table 4) with a study in Taiwan (Lin et al., 2010). The latter study was performed at sites with similar latitudes to ours and reported the diurnal variations of $T_{mrt}$ . In the study, the measured $T_{mrt}$ at Location A (Sky View Factors – SVF = 0.129) was ~30 °C in the morning and rose to ~50 °C at noon in summer. While at Location F, the measured $T_{mrt}$ (SVF = 0.808) was ~45 °C in the morning and rose to ~60 °C at noon in summer. These results were basically comparable with our predicted $T_{mrt}$ at in Table 4. For instance, our predicted $T_{mrt}$ at open-space were 42.5 °C (in the morning) and 58.8 °C (at noon) which were comparable to the results at Location F mentioned above. Our predicted $T_{mrt}$ for different Cases (SVF from 0.062 to 0.215) ranged from 34.8 °C to 35.4 °C which were comparable to 30 °C measured at Location A in the morning. Locations C and D for the Taiwan study had ground cover with grass and Location B was shaded with tall trees and thus these Locations were not selected for comparison, since the grass and tree effects (e.g. for cooling) were not considered in our study.

Table 4 also shows the calculated *PETs* at the street intersection and in the street canyon for different urban forms (or Cases) under the "no-heat" and "with-heat" scenarios. The case of "Open-space" was also added in the Table for a comparison of *PET* between an open space and a built environment. The calculated *PETs* produced sensible results when comparing with those listed in the human

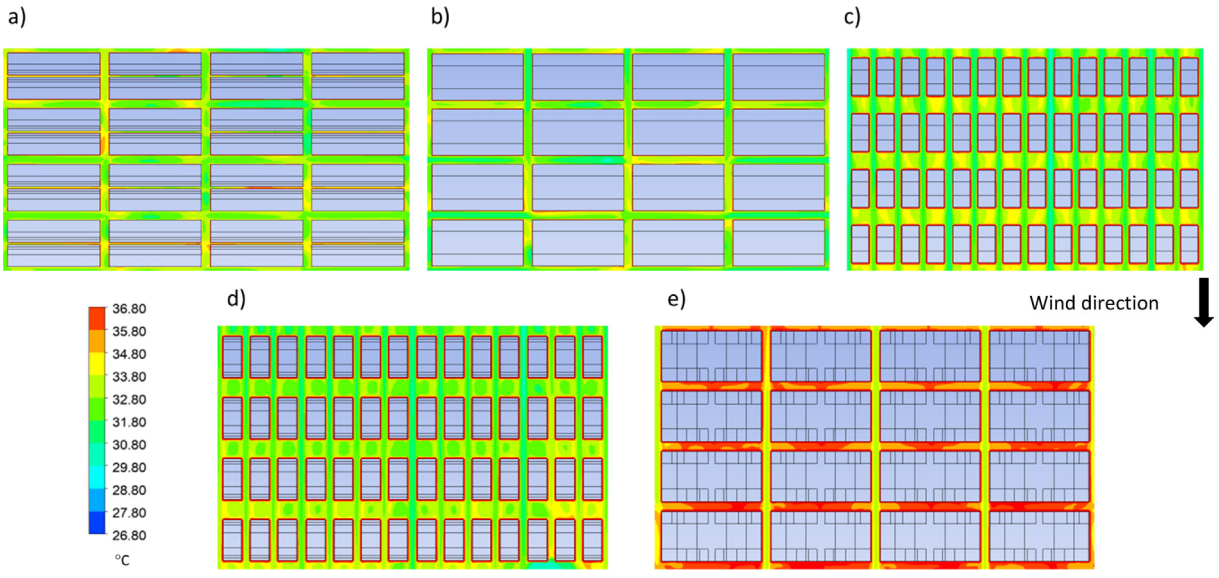


**Fig. 3.** Calculated pedestrian-level air temperatures for a) Case 1, b) Case 2, c) Case 5, d) Case 6a, and e) Case 7.

**Table 4**
Calculated $T_{mrt}$ (°C) and *PET* (°C) in different built environments under the "No-heat" and "With-heat" scenarios.

| | Street intersection[†] | Street canyon[†] |
|---|---|---|
| *"No-heat" scenario* | | |
| Case 1 | 35.4, 30.3 | 35.0, 31.6 |
| Case 2 | 35.1, 31.1 | 34.8, 32.3 |
| Case 5 | 34.7, 27.3 | 34.7, 27.3 |
| Case 6a | 34.8, 28.0 | 34.8, 28.3 |
| Case 7 | 34.6, 27.6 | 34.8, 31.9 |
| Open-space | 42.5, 32.7 | 42.5, 32.7 |
| *"With-heat" scenario* | | |
| Case 1 | 60.8, 45.6 | 61.7, 47.5 |
| Case 2 | 58.0, 42.6 | 62.0, 48.2 |
| Case 5 | 54.7, 38.2 | 56.5, 41.4 |
| Case 6a | 54.7, 38.2 | 55.6, 39.8 |
| Case 7 | 55.9, 40.5 | 64.1, 50.6 |
| Open-space | 58.8, 39.4 | 58.8, 39.4 |

[†] 1st and 2nd column data were $T_{mrt}$ and *PET* respectively.

thermal sensation categories (Table 2). For instance, during the summer, a receiver "felt" neutral or slightly warm in the morning (i.e., under the "no-heat" scenario), while the receiver "felt" hot or very hot at noon (i.e., under the "with-heat" scenario).

Under the "no-heat" scenario, the highest *PET* was calculated for the "Open-space" situation. The results indicated that when the buildings did not act as heat sources, the shading effects of the buildings effectively reduced the *PET* increase due to solar irradiance, despite the counter effects of wind blocking. For other cases, the receiver at the street intersection had similar *PETs* as those in the street canyon, except Case 7. The relatively large differences in *PET* for Case 7 between the street intersection and the street canyon were due to the relatively large reduction in the wind speed in the street canyon. The low wind speeds at the pedestrian level of the street canyon were due to the higher buildings and the solid structure near the receiver, although building porosity was included at some distances away from the receiver. The small increases in *PETs* in the street canyon were attributed to the combined effects of wind speed reduction and solar shading. Except for the "Open-space" situation, higher *PETs* were obtained for Case 1 and Case 2 due to the low wind availability within the long-building environment.

Under the "with-heat" scenario, increases in *PETs* by more than 10 °C relative to the "no-heat" scenario were found in most of the cases, except the "Open-space" situation. The *PET* differences obtained at the street intersection and in the street canyon became larger (from 1 to 10 °C). There were 3 (4) out of 5 cases where the calculated *PETs* were higher than the "Open-space" situation at the street intersection (in the street canyon). The results indicated that when the buildings acted as heat sources after insolation absorption, the increases in the air temperature at the street intersection and in the street canyon made an important contribution to the receiver *PET* despite the reduced effect of solar radiation on *PET* due to building shading. The differences (~10 °C) in the calculated *PET* at the street intersection and in the street canyon were the largest for Case 7, similar to the "no-heat" scenario. It was attributed to the resulted high temperature which was in turn due to the reduced wind speed in the street canyon. The *PET* differences for Cases 1 and 2 were still large due to the "long building" designs, especially for Case 2. It was noted that the building heights in Case 2 were 1.5 times as those in Case 1, which facilitated the heat accumulation within the street canyon. Due to the larger wind availability within the buildings to reduce the heat accumulation, Cases 5 and 6 gave lower *PETs*. The lower *PETs* for these cases relative to the "Open-space" situation were attributed to the shading effect for the former. To sum up, reduction of building lengths and increase in the low-level porosity were the most effective ways to reduce heat stresses at the pedestrian-level, mainly because of the production of well-ventilated environment by the two measures. It was consistent qualitatively with other studies. For instance, Amirtham et al. (2015) reported that *PET* was 5 °C lower at noon in a well ventilated environment (aspect ratio: < 1) relative to a poorly ventilated environment (aspect ratio: 3.1) in an urban area of India. In the current study, only the relationship between the OTC and urban forms was our focus. However, urban green infrastructure such as trees, grass covers, ponds and other water bodies which had important mitigating effects on the heat stress (Lindberg and Grimmond, 2011; Ballout et al., 2015; Lindberg et al., 2016; Lai et al., 2019) was not included. The effects of such infrastructure are obviously important for further study on the topic.

## 5. Concluding remarks

We coupled a CFD model to an OTC model to study the relationship between air flows, air temperature, building morphologies and outdoor human thermal comfort. The models were first validated by experimental data and measurements. The predicted $T_{mrt}$ and *PETs* respectively for different Cases and open-space were compared with the relevant measurements available in the literature and those listed in the human thermal sensation categories. The street-level *PETs* within different urban forms were then investigated and rationalized. Recommendations were made to reduce the *PETs* in terms of better building design - reduction of building lengths and increase in the low-level porosity were the most effective ways to reduce heat stresses at the pedestrian-level. However, such recommendations are likely to be applicable for tropical and sub-tropical areas (e.g. cities in southern China and Singapore) where heat stress is a major health issue. The effects of urban green infrastructure are suggested to be included for further study on the topic.

## Declaration of Competing Interest

The authors declare that they have no known competing financial interests or personal relationships that could have appeared to influence the work reported in this paper.

## Acknowledgment

We acknowledge Mr. Neon M. H. He at the Institute of Environment, Energy and Sustainability, Chinese University of Hong Kong for his contribution to the earlier preparation of the study.

## Appendix A. Supplementary data

Supplementary data to this article can be found online at https://doi.org/10.1016/j.scitotenv.2019.134516.

## References

Amirtham, L.R., Horrison, E., Rajkumar, S., 2015. Impact of Urban Morphology on Microclimatic Conditions and Outdoor Thermal Comfort-A Study In Mixed Residential Neighbourhood of Chennai, India. ICUC9-9th International Conference on Urban Climate jointly with 12th Symposium on the Urban Environment, Toulouse, France.
Allegrini, J., Dorer, V., Carmeliet, J., 2015. Influence of morphologies on the microclimate in urban neighbourhoods. J. Wind Eng. Ind. Aerod. 144, 108–117.
Andrade, H., Alcoforado, M.J., 2008. Microclimatic variation of thermal comfort in a district of Lisbon (Telheiras) at night. Theor. Appl. Climatol. 92, 225–237.
Asfour, O.S., 2010. Prediction of wind environment in different grouping patterns of housing blocks. Energ. Buildings 42, 2061–2069.
Ballout, A., Lacheheb, D.E.Z., Bouchahm, Y., 2015. Improvement of thermal comfort conditions in an urban space (Case Study: The Square of Independence, Sétif, Algeria). Eur. J. Sustain. Dev. 4, 407–416.

Berdahl, P., Bretz, S.E., 1997. Preliminary survey of the solar reflectance of cool roofing materials. Energ. Buildings 25, 149–158.
Chen, Y.C., Lin, T.P., Matzarakis, A., 2014. Comparison of mean radiant temperature from field experiment and modelling: a case study in Freiburg. Germany. Theor. Appl. Climatol. 118, 535–551.
Chu, A.K.M., Kwok, R.C.W., Yu, K.N., 2005. Study of pollution dispersion in urban areas using Computational Fluid Dynamics (CFD) and Geographic Information System (GIS). Environ. Modell. Softw. 20, 273–277.
Flaherty, J.E., Stock, D., Lamb, B., 2007. Computational fluid dynamic simulations of plume dispersion in urban Oklahoma City. J. Appl. Meteor. Climatol. 46, 2110–2126.
Fluent, 2006 FLUENT 6.3 user's guide – Chapter 12 Modelling Turbulence, Fluent Inc.
Guéritée, J., Tipton, M.J., 2015. The relationship between radiant heat, air temperature and thermal comfort at rest and exercise. Physiol. Behav. 139, 378–385.
Hiemstra, J.A., Saaroni, H., Amorim, Jorge H., 2017. The urban heat island: thermal comfort and the role of urban greening. In: Pearlmutter, D. (Ed.), The Urban Forest: Cultivating Green Infrastructure for People and the Environment. Springer International Publishing AG.
Hwang, R.L., Lin, T.P., Matzarakis, A., 2011. Seasonal effects of urban street shading on long-term outdoor thermal comfort. Build. Environ. 46, 863–870.
Lai, A., Maing, M., Ng, E., 2017. Observational studies of mean radiant temperature across different outdoor spaces under shaded conditions in densely built environment. Build. Environ. 114, 397–409.
Lai, D. et al., 2019. A review of mitigating strategies to improve the thermal environment and thermal comfort in urban outdoor spaces. Sci. Total Environ. 661, 337–353.
Lee, H., Mayer, H., 2016. Validation of the mean radiant temperature simulated by the RayMan software in urban environments. Int. J. Biometeorol. 60, 1775–1785.
Lin, T.P., Matzarakis, A., Hwang, R.L., 2010. Shading effect on long-term outdoor thermal comfort. Build. Environ. 45, 213–221.
Lindberg, F., Grimmond, C.S.B., 2011. Nature of vegetation and building morphology characteristics across a city: Influence on shadow patterns and mean radiant temperatures in London. Urban Ecosyst. 14, 617–634.
Lindberg, F., Onomura, S., Grimmond, C.S.B., 2011. Influence of ground surface characteristics on the mean radiant temperature in urban areas. Int. J. Biometeorol. 60, 1439–1452.
Louka, P. et al., 2001. Thermal effects on the airflow in a street canyon - Nantes '99 experimental results and model simulation. Proceedings of the third international conference on urban air quality, Loutraki, Greece.
Matzarakis, A., Rutz, F., Mayer, H., 2007. Modelling radiation fluxes in simple and complex environments—application of the RayMan model. Int. J. Biometeorol. 51, 323–334.
Matzarakis, A., Rutz, F., Mayer, H., 2010. Modelling radiation fluxes in simple and complex environments: basics of the RayMan model. Int. J. Biometeorol. 54, 131–139.
Mayer, H., Höppe, P., 1987. Thermal comfort of man in different urban environments. Theor. Appl. Climatol. 38, 43–49.
Menter, F.R., Kuntz, M., Langtry, R., 2003. Ten years of industrial experience with the SST turbulence model. In: Hanjalic, K., Nagano, Y., Tummers, M. (Eds.), Proc. Turbulence Heat and Mass Transfer, pp. 625–632.
MK, 2019 Wikipedia – Mong Kok. Available at: https://en.wikipedia.org/wiki/Mong_Kok (Date of access: 15 Aug 2019).
Morabito, M. et al., 2014. Environmental temperature and thermal indices: what is the most effective predictor of heat-related mortality in different geographical contexts? Sci. World J. 2014, 961750.
Nakamura, Y., Oke, T.R., 1988. Wind, temperature and stability conditions in an east-west oriented urban canyon. Atmos. Environ. 22, 2691–2700.
Perini, K., Magliocco, A., 2014. Effects of vegetation, urban density, building height, and atmospheric conditions on local temperatures and thermal comfort. Urban For. Urban Green. 13, 495–506.
Rose, A.L., 2010. Impact of urbanization on the thermal comfort conditions in the hot humid city of Chennai, India. Recent Advances in Space Technology Services and Climate Change (RSTS & CC-2010), Chennai, India.
Santamouris, M., 2015. Analyzing the heat island magnitude and characteristics in one hundred Asian and Australian cities and regions. Sci. Total Environ. 512–513, 582–598.
Sofia, T., Fredrik, L., Ingegärd, E., Björn, H., 2007. Different methods for estimating the mean radiant temperature in an outdoor urban setting. Int. J. Climatol. 27, 1983–1993.
Steeneveld, G.J. et al., 2011. Quantifying urban heat island effects and human comfort for cities of variable size and urban morphology in the Netherlands. J. Geophys. Res. 116, D20129.
Uehara, K., Murakami, S., Oikawa, S., Wakamatsu, S., 2000. Wind tunnel experiments on how thermal stratification affects flow in and above urban street canyons. Atmos. Environ. 34, 1553–1562.
van Hove, L.W.A. et al., 2015. Temporal and spatial variability of urban heat island and thermal comfort within the Rotterdam agglomeration. Build. Environ. 83, 91–103.
Wai, K.M. et al., 2017. Aerosol pollution and its potential impacts on outdoor human thermal sensation: East Asian perspectives. Environ. Res. 158, 753–758.
Wang, Y., Berardi, U., Akbari, H., 2016. Comparing the effects of urban heat island mitigation strategies for Toronto. Canada. Energ. Buildings 114, 2–19.
Yang, B., Olofsson, T., Nair, G., Kabanshi, A., 2017. Outdoor thermal comfort under subarctic climate of north Sweden – A pilot study in Umeå. Sustain. Cities Soc. 28, 387–397.
Yang, F., Qian, F., Lau, S.S.Y., 2013. Urban form and density as indicators for summertime outdoor ventilation potential: a case study on high-rise housing in Shanghai. Build. Environ. 70, 122–137.
Yang, W., Wong, N.H., Lin, Y., 2015. Thermal comfort in high-rise urban environments in Singapore. Procedia Engg. 121, 2125–2131.
Yuan, C., Ng, E., 2012. Building porosity for better urban ventilation in high-density cities – A computational parametric study. Build. Environ. 50, 176–189.